Available online at www.sciencedirect.com
ScienceDirect
Ceramics International 38 (2012) 153–158
CERAMICS INTERNATIONAL
www.elsevier.com/locate/ceramint

Chemical stability and electrochemical properties of $CaMoO_{3-\delta}$ for SOFC anode

H.-N. Im, S.-Y. Jeon, M.-B. Choi, H.-S. Kim, S.-J. Song *

Department of Materials Science and Engineering, Chonnam National University, 300 Yongbong-dong, Buk-gu, Gwangju, 500-757, Republic of Korea

Received 10 December 2010; received in revised form 11 April 2011; accepted 2 May 2011
Available online 1st July 2011

Abstract

In an effort to develop alternative anode materials based on mixed conducting ceramics capable of offering high mixed ionic–electronic conductivity, stability to redox cycles, and limited activity for carbon formation to Ni/YSZ cermets, $CaMoO_3$ ceramics for application as a solid oxide fuel cell (SOFC) anode material were synthesized as a function of temperature and oxygen partial pressure (pO_2). $CaMoO_3$ perovskite-dominant powders were obtained by reducing the $CaMoO_4$ showing a structure of orthorhombic unit cells with the following lattice parameters: $a = 5.45$ Å, $b = 5.58$ Å, and $c = 7.78$ Å. The equilibrium total conductivity of $CaMoO_3$, measured by DC 4-probe method in 5% H_2/balance N_2 condition ($pO_2 \approx 10^{-22}$ atm) at various temperatures, decreased with increasing temperature below 400 °C, indicating metallic properties with an activation energy of 0.028 eV. Between 400 °C and 600 °C, the equilibrium total conductivity slightly increased, and finally sharply decreased at 800 °C. The Mo metal precipitation during measurement was thermodynamically proved by the predominance diagram for $CaMoO_3$. Finally, a fuel cell with $CaMoO_3$ anode exhibited poor performance with a maximum power density of only 14 mW/cm^2 at 900 °C, suggesting that further research is needed to enhance the ionic conductivity and thus improve the catalytic properties.

Keywords: $CaMoO_3$; SOFC; Anode

1. Introduction

In recent years, solid oxide fuel cells (SOFCs) have been considered as the most efficient power generation system [1–4]. Due to their high operating temperatures, SOFCs offer several advantages such as low greenhouse gas emissions, high cell efficiency, and fuel flexibility. A general SOFC stack may be composed of three components: cermet anode, oxygen ion conducting electrolyte, and mixed conducting cathode [4,5]. In this component, the widely used Ni–yttria-stabilized zirconia (YSZ) cermet for anode shows good electrochemical performance when fed by hydrogen as a fuel [6,7]. However, the use of Ni-metal anodes in SOFCs has induced several technological problems such as carbon coking, Ni-coarsening, and sulfur poisoning when fed by natural gas, which is a more practically accessible fuel [8–10]. This has led to considerable efforts in developing alternative anode materials based on mixed conducting ceramics, especially high mixed ionic–electronic conductivity, stability to redox cycles, and limited activity for carbon formation to Ni/YSZ cermets. Among various kinds of oxide material, the perovskite structure has received great attention for SOFC electrodes due to its excellent electronic properties with considerable ionic conductivity [11–13]. According to a criterion for localized vs. collective d-electron behavior in transition-metal oxides with perovskite structure [14,15], $AMoO_3$ (A = Ca, Sr, Ba) perovskites containing Mo^{4+} cation have sufficient electron transfer energy to screen and cancel the electrostatic energy accompanied by the electron transfer. Among the these three perovskite compounds, $CaMoO_3$ has the highest conductivity at room temperature ($\sim 10^4$ S cm^{-1}), and its thermal expansion coefficients are very close to those of YSZ, which is widely used for SOFC electrolytes [16].

In this work, $CaMoO_3$ ceramics for application as an anode material for SOFC are synthesized as a function of temperature and oxygen partial pressure (pO_2). Their phase distribution, microstructure, electrical properties, and anode performance are studied in detail.

* Corresponding author. Tel.: +82 62 530 1706; fax: +82 62 530 1699.
E-mail address: song@chonnam.ac.kr (S.J. Song).

0272-8842/$36.00
doi:10.1016/j.ceramint.2011.05.155

2. Experimental

A typical method of $CaMoO_3$ powder preparation is the reduction of $CaMoO_4$ at elevated temperature. $CaMoO_4$ scheelite powders were first prepared by citric acid method. $CaCO_3$ (Aldrich, 99.99%), and $(NH_4)_6Mo_7O_{24}4H_2O$ (Aldrich, 99.99%) were dissolved in 10% citric acid. The mixed solution was dried at 120 °C for 12 h for complete dehydration and then heated at 800 °C for 10 h in air. To obtain perovskite $CaMoO_3$ powders, $CaMoO_4$ was reduced at various temperatures using H_2/N_2 forming gases. The obtained powders were characterized by X-ray diffraction (XRD; D/MAX Ultima III, Rigaku, Japan) equipped with a Cu target X-ray tube at a scan rate of 1°/min between scanning angles of (2θ) 10° and 90°. The obtained XRD patterns were refined using the Full-Prof program according to the Rietveld method. Thermogravimetric/differential thermal analysis (TG/DTA) was performed with SDT Q600 V8.0 Build 95 thermal analyzer at a heating rate of 3 K/min from room temperature to 1173 K in air with a flow rate of 100 cc/min. The pO_2 was monitored before and after the thermal analysis with a zirconia oxygen sensor. X-ray photoelectron spectroscopy (XPS) analysis was performed using a VG Multilab 2000 spectrometer (Thermo VG Scientific) in an ultra high vacuum with an unmonochromatized Mg Kα (1253.6 eV) source and a spherical section analyzer. Survey scan data and core peak data were collected using pass energies of 50 and 20 eV, respectively. No charge neutralization was used. The binding energy (BE) scale was calibrated from the hydrocarbon contamination using the C1s peak at 284.5 eV. All BEs obtained in this study were precise to within ±0.2 eV [17].

The total DC conductivity was measured by a standard, 4-probe method using a measurement system including a digital multimeter (Keithley 2700) combined with a programmable current source (Keithley 220) at the temperature range of 100–800 °C. For fuel cell testing, a $CaMoO_4$ anode and LSCF1982 cathode were screen printed onto a YSZ electrolyte surface (around 20 μm). The cell was sintered in air at 1050 °C for 2 h. The cells were attached to an alumina tube and reduced anode side. The cell was first annealed at 900 °C, in a 10% H_2 atmosphere with balance of N_2 for 2 h to prepare the perovskite $CaMoO_3$ anode. The impedance spectra of the electrochemical cell were recorded at open circuit voltage (OCV) over the frequency range 0.01 Hz–10 MHz with a Solartron 1260 Impedance Analyser. The ohmic resistance of the electrolyte and the anode (RV) was estimated from the high frequency intercept of the impedance curves and the overall electrode polarization (interface) resistance (RE) was directly measured from the differences between the low and high frequency intercepts on the extended impedance curves. The impedance responses were analyzed using an equivalent RC circuit method. The measurement was carried out in the temperature range of 700–900 °C. The *I–V* property of coin-cell was tested using a Solartron 1287 potentiostatic.

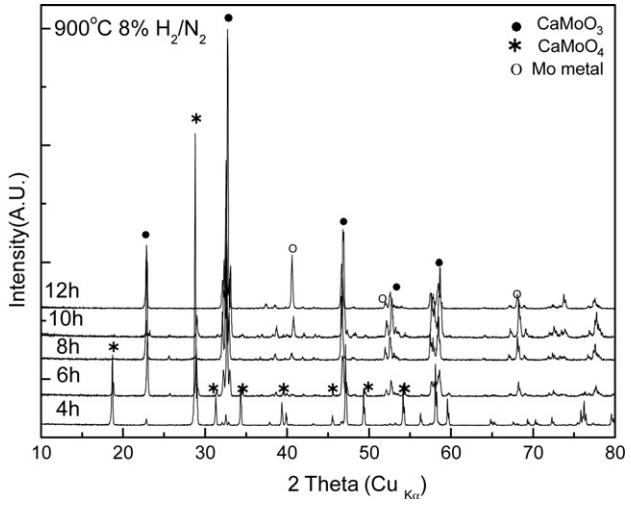

Fig. 1. Room temperature X-ray diffraction (XRD) patterns of $CaMoO_3$ annealed at 900 °C in 8% H_2/balance N_2 for various dwelling times.

3. Results and discussion

To obtain single phase $CaMoO_3$ powders, the reduction method for $CaMoO_4$ was applied at various temperatures using H_2/N_2 forming gases. The XRD pattern of the reduced $CaMoO_3$ compound as a function of dwelling time at 900 °C in 8% H_2/balance N_2 conditions is shown in Fig. 1. The results show a characteristic pattern of composite composed of $CaMo_4$ scheelite, $CaMoO_3$ perovskite, and Mo metal. As the dwelling time was increased from 4 h to 12 h, the content of the $CaMoO_4$ scheelite phase decreased and was completely reduced to $CaMoO_3$ and Mo after 10 h. No single phase $CaMoO_3$ perovskite powders were obtained, suggesting that the $CaMoO_3$ perovskite is not thermodynamically stable at the given pO_2 ($\approx 10^{-19}$ atm, 900 °C), in contrast to literature reports [18,19] (Table 1).

Another report on the preparation of $CaMoO_3$ perovskite powders examined the effect of changing the reduction thermodynamic condition [20]. In accordance with the method reported in that study, the $CaMoO_4$ was reduced at 1200 °C in 2% H_2/balance N_2 conditions for 10 h. The XRD pattern of the reduced $CaMoO_3$ compound still presented a trace of Mo metal, as shown in Fig. 2, but at a greatly reduced level compared with that shown in Fig. 1. The obtained XRD pattern was refined using the Full-Prof program according to the Rietveld method, and is also depicted in Fig. 2. Although the results of line profiling analysis may not have been completely reliable because of the relatively fast scan rate (1°/min), no peaks were detected except for a small Mo peak at around 38°. The refined

Table 1
Binding energies (eV) of Mo3d levels [23].

Assignt	Binding energy (eV)	
	$Mo3d_{3/2}$	$Mo3d_{5/2}$
Mo^{6+}	235.9	232.7
Mo^{5+}	234.6	231.4
Mo^{4+}	232.8	229.6
Mo^{3+}	232.0	228.8
Mo^{2+}	231.4	228.2
Mo^{0}	230.8	227.6

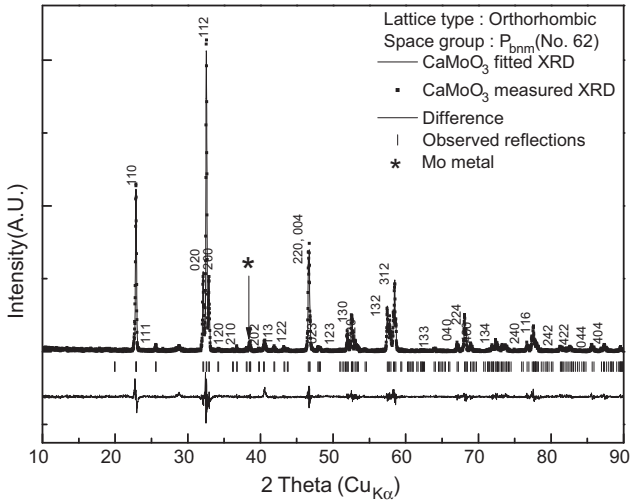

Fig. 2. Room temperature X-ray diffraction (XRD) patterns by reducing the $CaMoO_4$ at 1200 °C in 2% H_2/balance N_2 conditions for 10 h.

orthorhombic unit cell parameters for $CaMoO_3$ at ambient temperature were $a = 5.45$ Å, $b = 5.58$ Å, and $c = 7.78$ Å, which is in agreement with a previous report [21].

To elucidate the oxidation state of the Mo metal in the prepared $CaMoO_3$, XPS analysis was carried out and the results are shown in Fig. 3. Peaks for $Mo3p_{3/2}$ and $Mo3p_{5/2}$ were observed at 233.15 and 230.05 eV, respectively. These BE values correspond to the Mo^{4+} state and practically do not differ from those previously reported [22,23]. The BEs of an electron corresponding to Mo^{6+} in $CaMoO_4$ at 232.6 and 235.8 eV were not observed, suggesting that no $CaMoO_4$ phase remained in scheelite form.

After $CaMoO_3$ was sintered at 1200 °C in 2% H_2/balance N_2 conditions for 10 h, its equilibrium total conductivity in 5% H_2/balance N_2 condition ($pO_2 \approx 10^{-22}$ atm) was measured at various temperatures by DC 4-probe method and the results are shown in Fig. 4. The equilibrium total conductivity of $CaMoO_3$ decreased with increasing temperature below 400 °C, indicating metallic properties with an activation energy of 0.028 eV, which is consistent with a previous report [18]. Between 400 °C and 600 °C, the equilibrium total conductivity slightly increased, indicating a semiconductor-type behavior, and finally sharply decreased at 800 °C. As shown in the inserted figure in Fig. 4, the conductivity at 800 °C did not reach any equilibrium within 50 h but rather continued to decrease.

After measurement up to 800 °C for 50 h, the fractured surface of the $CaMoO_3$ was examined by SEM micrographs, as shown in Fig. 5b, and compared with the as-sintered $CaMoO_3$ specimen in Fig. 5a. Interestingly, many nanocrystalline grains were uniformly precipitated within the grains of the post-measurement specimen and totally disconnected $CaMoO_3$ grains were also observed. The XRD pattern of the post-measurement $CaMoO_3$ specimen shown in Fig. 5c clearly reveals the Mo metal precipitation. The further TG/DTA result suggests possible phase separation by monitoring the significant weight decrease above 800 °C [24]. Therefore, an attempt was made to determine the thermodynamically stable regime of $CaMoO_3$. The predominance diagram for the Ca–Mo–O system depicted in Fig. 6 was attained by using the minimum-free-energy formation method. As shown in Fig. 6, with a fixed activity of CaO vapor at 10^{-22} atm, the $CaMoO_3$ phase started to deviate from its stability regime and the Mo metal phase became thermodynamically stable at the conductivity measurement condition at 800 °C in pO_2 of 10^{-22} atm. Even the sintering condition of $CaMoO_3$ belonged to the Mo phase-dominant regime, although the reduction kinetics of $CaMoO_3$ may not be fast enough. These results led us to conclude that $CaMoO_3$ may not be thermodynamically

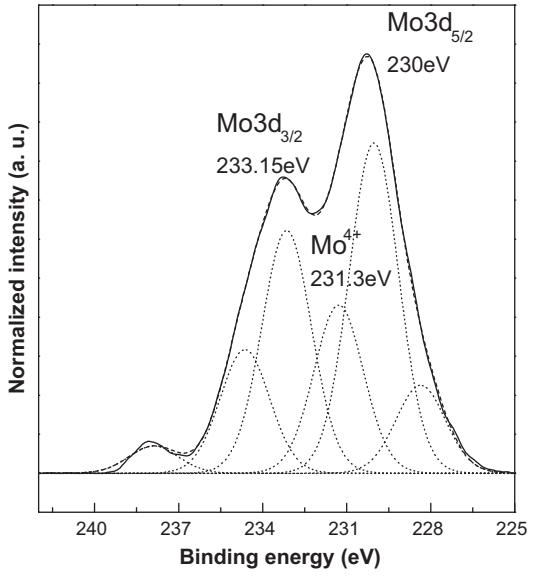

Fig. 3. X-ray photoelectron spectroscopy (XPS) spectra of the Mo3d doublet prepared at 1200 °C in 2% H_2/balance N_2 conditions for 10 h.

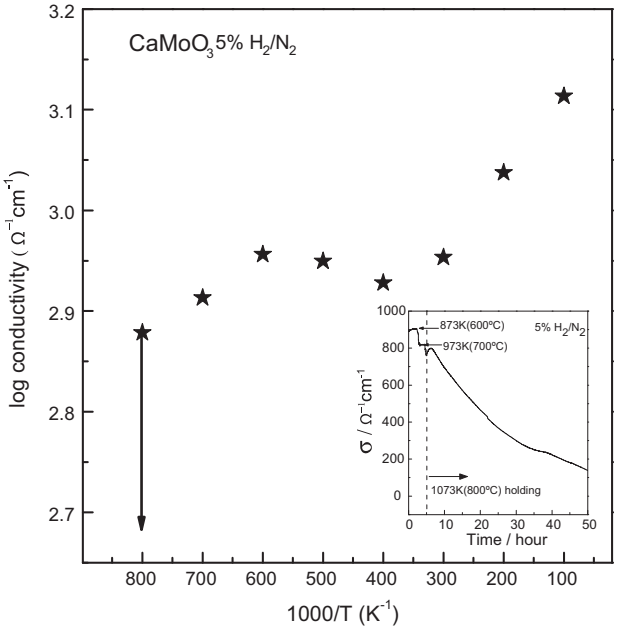

Fig. 4. Total conductivity of $CaMoO_3$ as a function of temperature measured by 4-probe DC conductivity method.

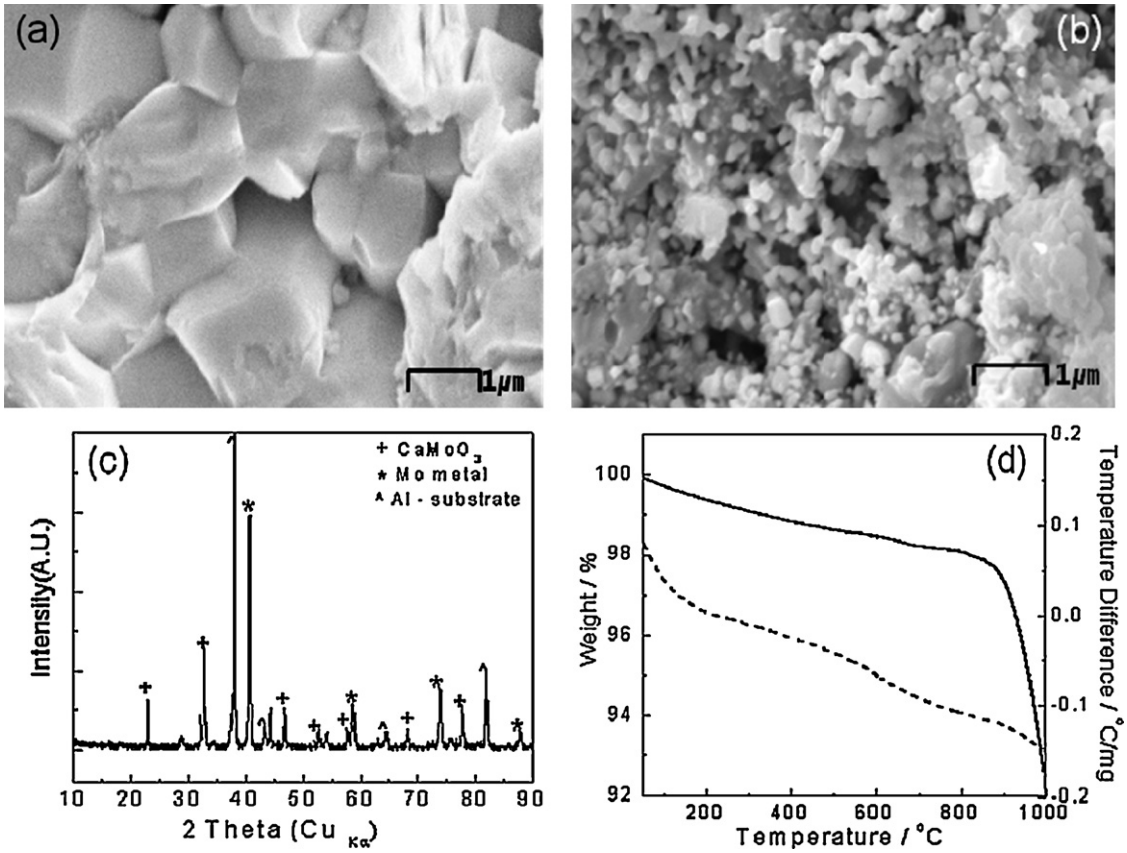

Fig. 5. Scanning electron micrographs (SEM) of the polished fracture surface of $CaMoO_3$ (a) sintered at 1200 °C in 2% H_2/balance N_2 conditions, and (b) after conductivity measurement in 5% H_2/balance N_2 condition. (c) XRD patterns of post-measurement $CaMoO_3$ specimen, and (d) thermogravimetric/differential thermal analysis (TG/DTA) curve for $CaMoO_3$.

stable at fuel cell operation conditions, and even the reported preparation methods of single phase perovskite $CaMoO_3$ powders may not be correctly performed.

To investigate the anode performance of $CaMoO_3$, the *I–V* and *I–P* relationship of the cell was tested under air and H_2 flowing condition. Fig. 7a shows the *I–V* and *I–P* curves of the cell with an ≈20 μm-thick LSCF1982 cathode and $CaMoO_3$ anode with a 1.4 mm-thick YSZ electrolyte, as shown in Fig. 7b. The $CaMoO_3$ anode was prepared by sintering in air at 1050 °C for 2 h followed by annealing $CaMoO_4$ at 900 °C, 10% H_2/balance N_2 conditions for 2 h. The fuel cell performance was then tested from 900 °C after 30 min at the target temperature to minimize the Mo precipitation. OCV at 900 °C was around 1.2 V, suggesting that the fuel leakage of our cell may have been negligible. However, this fuel cell with $CaMoO_3$ anode poor performance with a maximum power density of only 14 mW/cm^2 at 900 °C, due to the thick electrolyte and also the poor anodic performance that was attributed both to the negligible ionic conductivity and the decomposition of $CaMoO_3$. One should notice that the equilibrium *I–V* measurement could not be achieved above 800 °C because of the time-depending CMO_3 phase decomposition. Electrochemical impedance spectroscopy (EIS) experiments were conducted in a three-point configuration where the reference Pt-electrode was wound around the YSZ electrolyte and impedance spectra were obtained as a function of temperature, as shown in Fig. 8. The ohmic resistance calculated from the high frequency intercept was around 15 S cm^{-1}, which is much higher than YSZ electrolyte, suggesting that the insulating phase may form during high temperature operation as expected from equilibrium conductivity measurement.

The EIS curves were mainly governed by the IR resistance, charge transport polarization, and activation polarization. Two prominent semicircular features became obvious. The relative

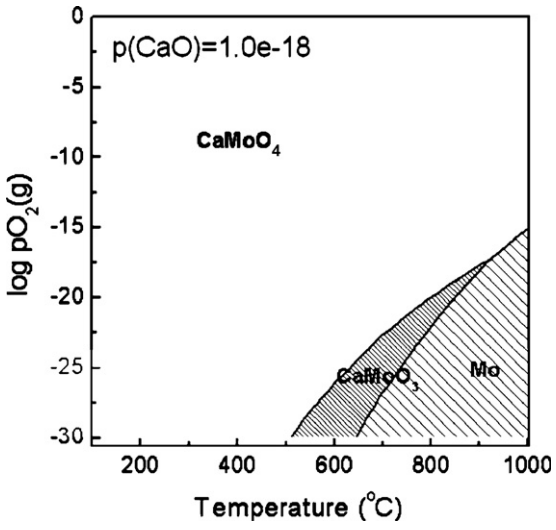

Fig. 6. Predominance phase diagram of $CaMoO_3$.

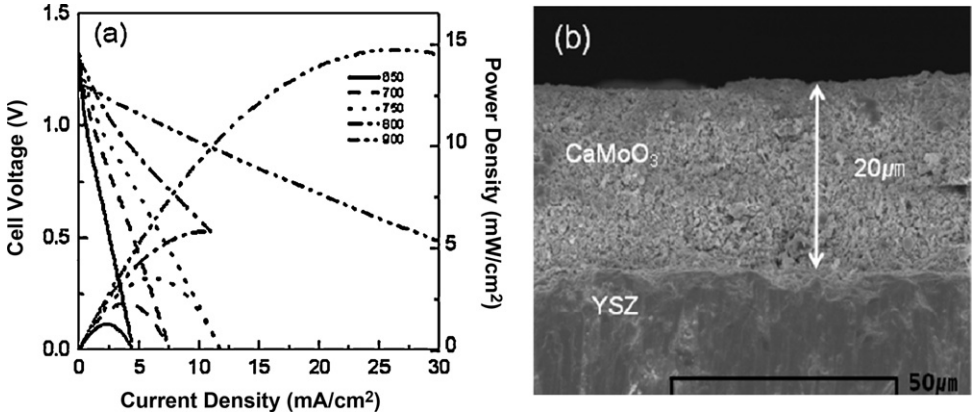

Fig. 7. (a) Voltage and (b) powder density versus current density of the cell with LSCF1982 cathode, 1.4 mm-thick YSZ electrolyte, and ≈22 μm-thick $CaMoO_3$ anode.

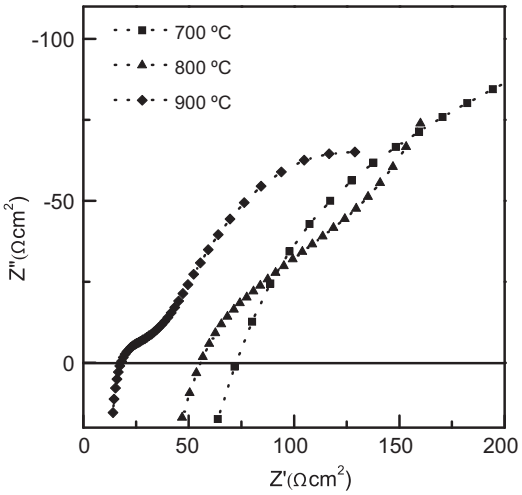

Fig. 8. Cell impedance spectra obtained at open circuit voltage (OCV) for different temperatures.

magnitude of the high frequency first arch decreased with temperature, which was related to the anode charge transport overpotential. The low frequency second arch may have been influenced by the activation overpotential. Calculated from the EIS measurements, the anode area specific resistance of the cell was 270 Ωcm^2 at 900 °C. These study results may suggest that the catalytic properties of high electron conducing $CaMoO_3$ can be further enhanced to a degree suitable for SOFC anode application below 800 °C by improving its ionic conductivity and microstructure with forming composite electrode with oxygen ion conducting phase.

4. Conclusions

$CaMoO_3$ perovskite-dominant powders were obtained by reducing the $CaMoO_4$ at 1200 °C in 2% H_2/balance N_2 conditions for 10 h. The refined orthorhombic unit cell parameters for $CaMoO_3$ at ambient temperature were a = 5.45 Å, b = 5.58 Å, and c = 7.78 Å. The equilibrium total conductivity of $CaMoO_3$, measured by DC 4-probe method in 5% H_2/balance N_2 condition ($pO_2 \approx 10^{-22}$ atm) at various temperatures, decreased with increasing temperature below 400 °C, indicating metallic properties with an activation energy of 0.028 eV. Between 400 °C and 600 °C, the equilibrium total conductivity slightly increased, indicating a semiconductor-type behavior, and finally sharply decreased at 800 °C. The XRD pattern of the post-measurement $CaMoO_3$ specimen clearly showed the Mo metal precipitation. A fuel cell with $CaMoO_3$ anode exhibited poor performance with a maximum power density of only 14 mW/cm^2 at 900 °C, due to the thick electrolyte and also the poor anodic performance that was attributed to the negligible ionic conductivity of $CaMoO_3$.

Acknowledgement

This work was supported by Solid Oxide Fuel Cell of Mew & Renewable Energy R&D Program (20093021030010) under the Korea Ministry of Knowledge Economy (MIKE)

References

[1] S.P. Simner, J.F. Bonnett, N.L. Canfield, K.D. Meinhardt, J.P. Shelton, V.L. Sprenkle, J.W. Stevensonm, Development of lanthanum ferrite SOFC cathodes, J. Power Sources 113 (2003) 1–10.
[2] A. Atkinson, S. Barnett, R.J. Gorte, J.T.S. Irvine, A.J. Mcevoy, M. Mogensen, S.C. Singhal, J. Vohs, Advanced anodes for high-temperature fuel cells, Nat. Mater. 3 (2004) 17–27.
[3] S.P.S. Badwal, K. Foger, Solid oxide electrolyte fuel cell review, Ceram. Int. 22 (1996) 257–265.
[4] S.P. Jiang, S.H. Chan, A review of anode materials development in solid oxide fuel cells, J. Mater. Sci. 39 (2004) 4405–4439.
[5] J.W. Fergus, Oxide anode materials for solid oxide fuel cells, Solid State Ionics 177 (2006) 1529–1541.
[6] O. Yamamoto, Solid oxide fuel cells: fundamental aspects and prospects, Electrochim. Acta 45 (2000) 2423–2435.
[7] S.C. Singhal, Solid oxide fuel cells for stationary, mobile, and military applications, Solid State Ionics 152–153 (2002) 405–410.
[8] Y. Matsuzaki, I. Yasuda, The poisoning effect of sulfur-containing impurity gas on a SOFC anode, Solid State Ionics 132 (2000) 261–269.
[9] W.Z. Zhu, S.C. Deevi, A review on the status of anode materials for solid oxide fuel cells, Mater. Sci. Eng. A362 (2003) 228–239.
[10] S. McIntosh, J.M. Vohs, R.J. Gorte, Role of hydrocarbon deposits in the enhanced performance of direct-oxidation SOFCs, J. Electrochem. Soc. 150 (2003) A470–A476.

[11] Chunwen Sun, Ulrich Stimming, Recent anode advances in solid oxide fuel cells, J. Power Sources 171 (2007) 247–260.
[12] H. Yokokawa, N. Sakai, T. Horita, K. Yamaji, Recent developments in solid oxide fuel cell materials, Fuel Cells 1 (2001) 117–131.
[13] J.B. Goodenough, Covalency criterion for localized vs collective electrons in oxides with the perovskite structure, J. Appl. Phys. 37 (1966) 1415–1422.
[14] J.B.Goodenough, J.M.Longo, Landolt-Borstein Zahlenwerte und Funktionen, New Series BdIII/4a (1970).
[15] G.H. Bouchard, M.J. Sienko, Magnetic susceptibility of barium molybdate(iv) and strontium molybdate(IV) in the range 2–300 K, Inorg. Chem. 7 (1968) 441–443.
[16] S. Hayashi, R. Aoki, T. Nakamura, Metallic conductivity in perovskite type compounds $AMoO_3$ (A = Ba, Sr, Ca) down to 2.5 K, Mater. Res. Bull. 14 (1979) 409–413.
[17] H.N. Im, M.B. Choi, S.Y. Jeon, S.J. Song, Structure, thermal stability and electrical conductivity of $CaMoO_{4+d}$, Ceram. Int. 37 (2011) 49–53.
[18] K. Kamata, T. Nakamura, T. Sata, Sysnthesis and properties of the metallic molybdate(IV) $CaMoO_3$, Chem. Lett. 1 (1975) 81.
[19] K. Kamata, T. Nakamura, T. Sata, Mater. Res. Bull. 10 (1975) 373.
[20] A. Aguaderoa, C. de la Calle, J.A. Alonso, D. Pérez-Coll, M.J. Escudero, L. Daza, Structure, thermal stability and electrical properties of $Ca(V_{0.5}Mo_{0.5})O_3$ as solid oxide fuel cell anode, J. Power Sources 192 (2009) 78–83.
[21] C. de la Calle, J.A. Alonso, M. García-Fernández, V. Pomjakushin, Neutron diffraction study and magnetotransport properties of stoichiometric $CaMoO_3$ perovskite prepared by a soft-chemistry route, J. Solid State Chem. 79 (2006) 1636–1641.
[22] G.T. Kim, T.K. Park, H. Chung, Y.T. Kim, M.H. Kwon, J.G. Choi, Growth and characterization of chloronitroaniline crystals for optical parametric oscillators, Appl. Surf. Sci. 152 (1999) 35–43.
[23] J.F. Moulder, W.F. Sickle, P.E. Sobol, K.E. Bomben, Handbook of X-ray Photoelecteron Spectroscopy, Physical Electronics, Minnesota, 1995.
[24] W.H. McCarroll, R. Ward, L. Katz, Ternary oxides of tetravalent molybdenum, J. Am. Chem. Soc. 78 (1956) 2909–2910.